Mesoscale Wind Signatures along the Carolina Coast

ALLEN J. RIORDAN AND YUH-LANG LIN

Department of Marine, Earth and Atmospheric Sciences, North Carolina State University, Raleigh, North Carolina

(Manuscript received 7 June 1991, in final form 26 March 1992)

ABSTRACT

Coastal winds immediately offshore of North and South Carolina often exhibit a mesoscale diffluent–confluent pattern that appears to be governed by the coastal configuration and oceanic thermal field. The stationary pattern roughly parallels the coastline within 50 km of shore during winter when synoptic-scale conditions support northerly winds. Data obtained during the Genesis of Atlantic Lows Experiment (GALE) are statistically analyzed to document the surface winds in this offshore zone. Several specific examples of the mesoscale pattern are presented and compared with results from a simple theoretical model with diabatic heating.

For an inviscid flow over an isolated bell-shaped heat source, the air parcels rise in the vicinity of the heating region and descend on both the upstream and downstream sides. A confluent zone is produced in the vicinity of the heat source. With an idealized heat source resembling the observed pattern of sensible heat flux, the flow pattern is similar to that observed. Frictional effects are shown to be negligible. Thus, results from the simple theoretical model suggest that diabatic heating is largely responsible for the observed flow pattern.

1. Introduction

Eastern North Carolina and adjacent coastal waters provide a setting conducive to the development of surface low pressure systems that often adversely affect much of the east coast of the United States and the western Atlantic (Whittaker and Horn 1982; Dirks et al. 1988; Hadlock and Kreitzberg 1988). Some of these lows deepen rapidly as major "bombs," with central-pressure falls of at least 10 mb $(6\ h)^{-1}$ for at least 6 h. For example, during the field phase of the Experiment on Rapidly Intensifying Cyclones over the Atlantic (ERICA), which included the period from 1 December 1988 through 28 February 1989, eight low centers first formed within 200 km of Cape Hatteras, North Carolina. These storms represent three out of the four strongest cyclones studied during ERICA, which, in fact, exceeded the bomb deepening rate.

Coastal fronts in the mid-Atlantic region are often precursors of cyclogenesis (Austin 1941; Bosart and Lin 1984; Uccellini et al. 1987). In recent results from GALE, Doyle and Warner (1990) and Riordan (1990) documented the structure and evolution of a coastal front and described the importance of associated mesoscale processes, particularly those arising from strong gradients in both sea surface temperature (SST) and land–sea temperature fields.

Associated with the coastal front, zones of persistent surface confluence and diffluence located offshore immediately west of the frontal surface were described by Riordan (1990). In that case study, physical and circumstantial evidence suggested that these zones influence the evolution and normal westward progression of the front. For example, the front did not move smoothly past the topographically fixed diffluent and confluent wind fields. Rather, it appeared to avoid the diffluent region and to reinforce itself along the confluent zone. In general, in the case of the Carolina coastal front where the diffluent zone lies east of the confluent area, a front propagating from farther offshore may tend to jump from just east of the diffluent zone to the confluent area at the immediate shoreline.

In a numerical study of New England coastal frontogenesis, Ballentine (1980) suggested that the effect of heat fluxes from the ocean is important. This same effect may play a significant role in determining the flow field in the vicinity of the coastal front. Low-level sensible heating has also been shown to have important impact on mesoscale phenomena, such as heat island, sea breeze, and coastal cyclogenesis (e.g., Hsu 1987; Lin 1990). Therefore, it is meaningful to include the effects of low-level diabatic heating when attempting to describe the flow in the region.

The purpose of this study is to examine the diffluent–confluent wind regime, to determine under what conditions it is found, and to explore its physical cause. GALE data will be used, since because of its resolution, it affords a unique opportunity to observe the mesoscale wind field.

2. Data

The locations of key fixed observing sites used in this study are illustrated in Fig. 1. In addition, mobile

Corresponding author address: Dr. Allen J. Riordan, Department of Marine, Earth and Atmospheric Sciences, North Carolina State University, Box 8208, Raleigh, NC 27695-8202.

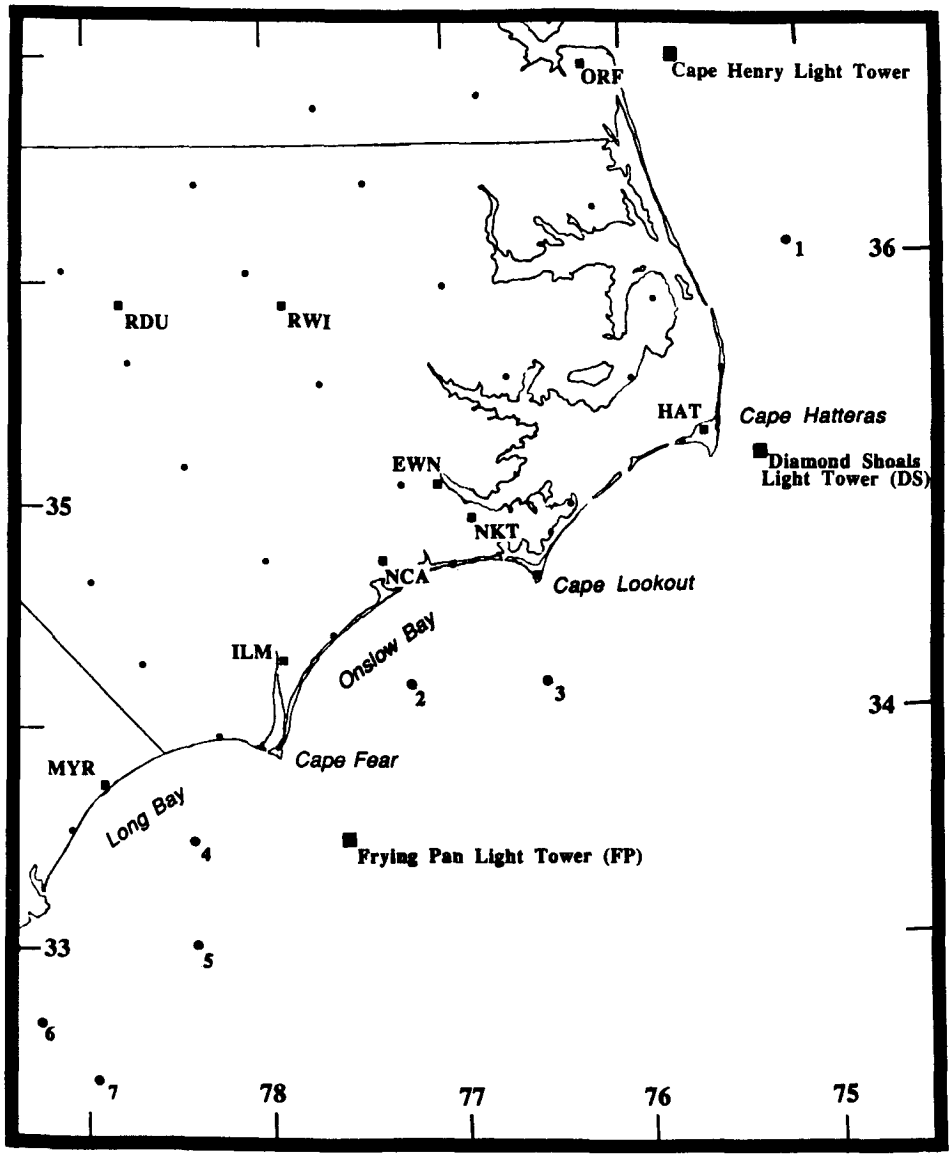

FIG. 1. Locations of fixed observing sites and key geographical reference points. Over land, small dots represent PAM II sites and large squares represent routine National Weather Service, Coastal Marine Automated Network (C-MAN), and military observing sites. Over water, squares represent C-MAN navigational light towers and numbered dots represent GALE buoys.

platforms including the R/V *Cape Hatteras* and the NCAR King Air research aircraft provided data for case studies presented.

The measurements were obtained from a wide assortment of systems. For example, among the fixed platforms, the systems include the Portable Automated Mesonet (PAM II) with stations reporting at 5-min intervals, a buoy network reporting hourly or half-hourly, and ship-of-opportunity data reporting at synoptic times. In addition, fixed oceanic platforms include truly stationary navigational light towers, which measure variables at heights of up to 47 m above the surface. On the other hand, buoys that also provide data are subject to wave motion and measure variables at only about 4 m above the surface.

Since this study relies on a synthesis of data from such a variety of systems, several procedures were used in data processing, including statistical and field intercomparisons, adjustments for differences in platform height, and temporal smoothing. These procedures are discussed in this section.

At Frying Pan Light Tower (FP), twin wind instruments were mounted 5.3 m above the roof of the lantern room, a closed tower structure projecting above a flat flight deck. This location placed both instruments 21.3 m above the flight deck and 44 m above mean

TABLE 1. Intercomparison of data from the R/V *Cape Hatteras* (RVC) and Frying Pan Light Tower (FP) for 9 April 1986.

	Sea temperature (°C)		Air temperature (°C)		Wind speed (m s^{-1})		Wind direction (deg)	
Time (UTC)	RVC	FP	RVC	FP	RVC	FP	RVC	FP
1300	21.5	—	16.5	16.7	16	21	335	340
1400	21.6	—	15.6	15.6	14	19	351	330
1500	21.3	—	16.0	15.5	12	22	350	330
1600	21.4	—	16.0	15.6	14	19	342	340
1700	21.3	—	15.3	—	14	—	340	—
1800	21.3	—	15.5	15.2	14	10	322	310
1900	21.2	—	16.1	15.8	12	18	307	290
2000	20.7	—	16.7	16.5	14	19	314	300
2100	20.7	—	17.5	16.5	14	21	299	300
2200	20.3	—	16.8	16.7	14	21	291	290

sea level. Wind studies by Thornthwaite et al. (1965) for this type of structure show that, while there may be some distortion of the flow regime due to the platform structure, for the instrument location described above, the distortion of the wind direction is probably negligible.

On 9 April 1986, the R/V *Cape Hatteras* was dispatched to FP for a 10-h wind intercomparison. The ship was positioned within sight of the tower and oriented with the ship's bow directed into the wind throughout the period. Results are presented in Table 1. The wind directions averaged 323° versus 314° at the ship and tower, respectively. The largest simultaneous difference was 21°. Wind speeds averaged 6 m s^{-1} greater at the tower, as might be expected given the 27-m height difference between the sensors.

Other field comparisons included ship–buoy and aircraft–buoy checks. Of particular interest are comparisons involving buoys 2 and 4 during north winds, since this study shows anomalous behavior at these two sites during such conditions. Ship–buoy comparisons showed reasonable agreement, as shown, for example, in Table 2. Unfortunately, only buoy 2 could be checked frequently, and all comparisons were made during light winds.

On 24 February 1986, the NCAR King Air research aircraft, flying at an altitude of about 150 m, passed just south of buoy 5. The comparison of wind measurements from these two platforms, plus surrounding surface sites, is illustrated in Fig. 2. The comparison is very good, but again, light and variable wind conditions prevail.

Since field comparisons between buoys and more controlled instrumentation were not available for moderate winds, considerable attention was paid to checking data quality during postprocessing. One noted characteristic of data from buoys 1, 2, 4, 5, 6, and 8 was the temporal variability of wind direction. For example, Fig. 3 illustrates the direction measured at buoy 1 and that from Diamond Shoals Light Tower located about 110 km to the south-southwest. Measured wind speeds for this period varied from 6 to 12 m s^{-1} at the buoy.

Since all six buoys are of similar design (Raman and Riordan 1988) and all showed similar variability, its likely cause is wave-induced motion. Because of power limitations, wind directions were not averaged, but were sampled instantaneously. To reduce effects of buoy motion, vanes were oil damped to suppress rapid oscillations, and the buoys were fitted with air foils to provide additional stability. Nevertheless, half-hourly directions varied within plus or minus 20° during most sea conditions.

To minimize resulting noise in the data, a centered five-point filter with weights 0.06, 0.25, 0.38, 0.25, and 0.06 was used to produce a more representative estimate of wind direction for the six buoys.

Finally, since differences in wind-sensor height were

TABLE 2. Intercomparison of measurements from research vessels *Cape Hatteras* and *Endeavor* with buoy 2. Comparisons were made for times when the ships were within sight of buoy 2.

		Ship		Buoy	
Date	Time (UTC)	Wind speed (m s^{-1})	Wind direction (deg)	Wind direction (deg)	Time (UTC)
11 December 1985	1353	1.5	330	314	1400
9 January 1986	1615	3.3	062	040	1630
	1636	1.5	352		
17 January 1986	0900	1.5	250	260	0900
31 January 1986	2000	1.4	125	140	2000

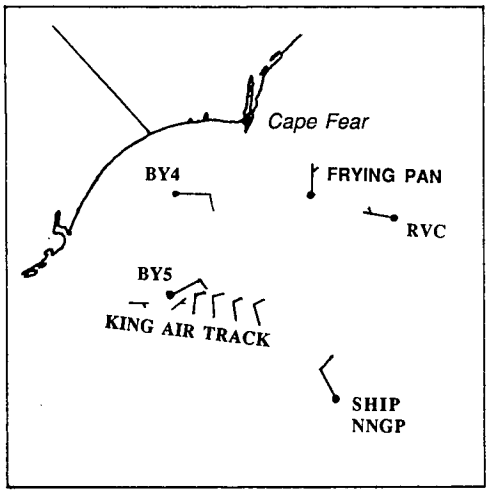

FIG. 2. Comparison of King Air and buoy 5 wind data for 24 February 1986.

sometimes large, several methods for reducing winds to a standard height of 10 m were considered. Static stability and thermal advection affect the change of both wind speed and direction with height. For this discussion, a simple method was used that neglects the effects of stability, since the required SSTs were not available for all sites.

The average wind speed at 10 m u_{10} was computed from the wind speed at height z, u_z, from

$$u_{10} = u_z\left[\ln\left(\frac{10}{z_0}\right) - \ln\left(\frac{z}{z_0}\right)\right]. \quad (1)$$

An initial guess of $z_0 = 5 \times 10^{-4}$ m was provided. From the neutral-drag-coefficient formula from Large and Pond (1982), namely, $C_{DN} = (0.049 + 0.065u_{10}) \times 10^{-3}$, and from the log-profile law and the definition of C_{DN}, namely, $C_{DN} = u^{*2}/u_{10}^2$, it is possible to compute a new z_0. Through Eq. (1) a new u_{10} was computed, and the process was repeated. The resulting iteration converges to a final value in only a few steps. Since C_{DN} depends on wind speed only for winds of greater than or equal to 10 m s^{-1} (Large and Pond 1982), we further specified that if the final value for u_{10} was less than 10.0 m s^{-1}, then $u_{10} = 11.55u_z[\ln(z/z_0)]^{-1}$, where $z_0 = 9.67 \times 10^{-5}$ m. The latter essentially specifies that C_{DN} is constant at 1.14×10^{-3} for low wind speeds.

All wind measurements presented in this study have been modified according to the procedures described previously. Thus, wind speeds have been adjusted to a standard height, and wind directions obtained from buoys have been smoothed. The effects of stability on wind speed and direction were not included. The resulting errors are probably small, however, ranging within a few percent for speed and 10° for direction. The latter is probably small because strong cold advection present in nearly all cases considered here produces a backing of the wind vector with height, which minimizes the normal veering due to friction (See Lettau 1950, 1962, for example).

3. Statistical sorting

The period from 15 January through 24 February 1986, when all PAM II and most buoy data were continuously available, formed the primary dataset. In this set, the hourly observations were grouped according to wind direction at two anchor points: Diamond Shoals Light Tower and FP. Times when the wind direction at both sites was between 340° and 50°, and when the wind speed at Diamond Shoals was at least 5 m s^{-1}, were selected for further study.

In all, 150 h, or 15% of the total GALE period, met the selection criteria. Most of the selected hours occurred in five episodes ranging in duration from 16 to 60 h. Resulting wind roses for all stations with at least 80% complete data for the selected hours are illustrated in Fig. 4. Here the directional percent frequency is plotted as a vector with each line representing a vector directed away from each site. At PAM II sites, wind directions were not included for wind speeds of less than 2 m s^{-1}.

The immediately obvious feature of Fig. 4 is the apparent diffluence of the flow east of buoys 2 and 4 located near the coast in Onslow Bay and in Long Bay. Here the nearshore winds appear to follow the coastline and do not resemble the more northerly flow in which they are embedded.

For some of the offshore sites, enough data were available to permit a more detailed examination of the pattern. For example, extension of the primary dataset back to 1 January yielded 247 h that meet the wind criteria. For this period, the mean difference in wind direction between buoy 4 and FP averaged 28° with a standard deviation of 18°. The streamlines at the two sites were parallel or confluent for only 21 h (9% of the sample).

In Onslow Bay, where the most complete record exists (buoys 2 and 3), the air temperatures were warmer

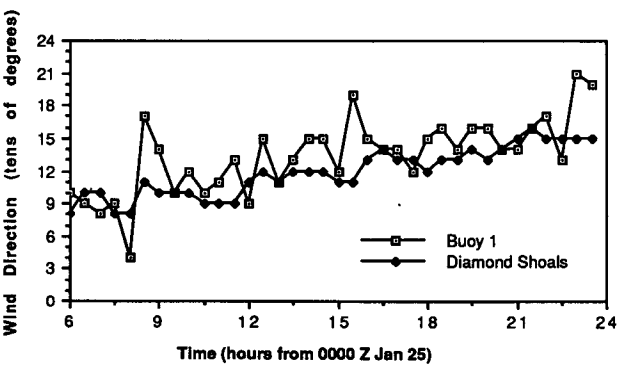

FIG. 3. Comparison of wind directions measured at buoy 1 with those reported from Diamond Shoals Light Tower.

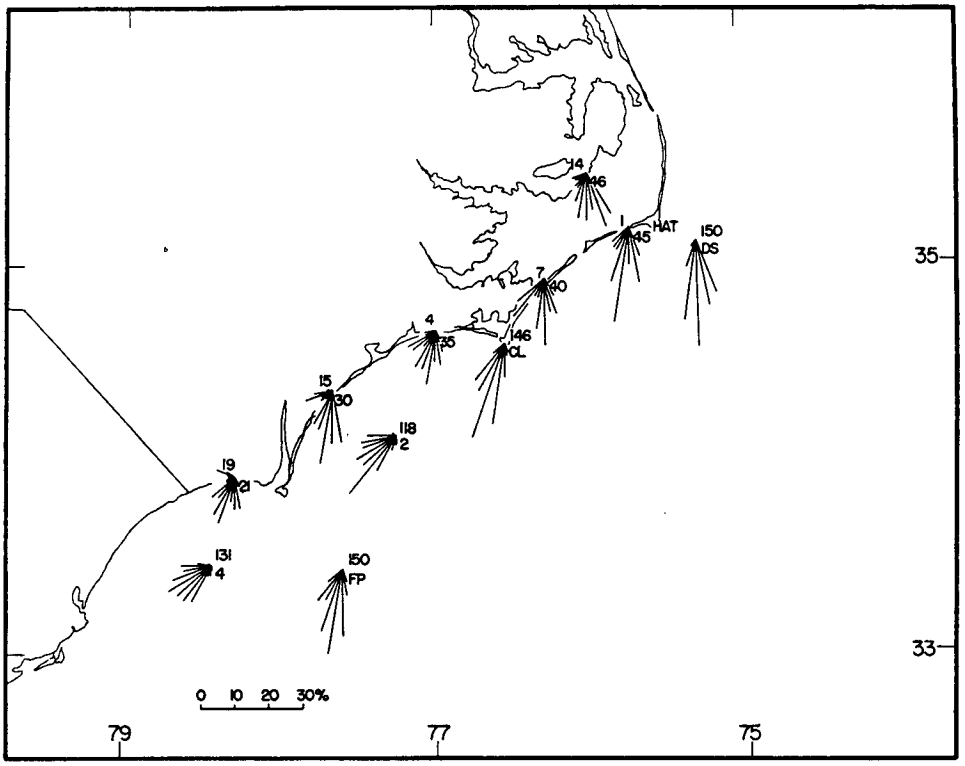

FIG. 4. Wind-direction frequency (%) for all times when the wind direction at both Diamond Shoals and Frying Pan Light Towers (DS and FP, respectively) was between 340° and 50° and for which the wind speed at DS was at least 5 m s^{-1}. Roses represent vectors directed outward from each site location.

than the sea temperatures in all but 4% of the 247 h, and all of these occurred at buoy 2 where the water temperatures were colder than at buoy 3. At the latter site, the air was colder than the water at all times. Thus, an upward flux of sensible heat is almost invariably present during northerly flow. This is certainly not surprising considering the season and the setting, but as will be seen hereafter, the upward flux may be very important in governing the shape of the flow pattern.

Examination of wind directional differences between buoy 4 and FP for other wind sectors showed no significant difference, thus ruling out a systematic measurement error as the probable cause. For example, for 437 h at FP, the wind direction was greater than 50° but less than 350°, and the wind speed was at least 5.0 m s^{-1}. For this subset, the most frequent directional sector (290 h) was from 190° through 270°. The mean difference in wind direction between the tower and buoy 4 for this sector was 9.5° with a standard deviation of 16.2°—hardly a significant difference. For other sectors, differences were even less.

The persistence and some sense of the spatial dimension of the diffluent pattern for northerly winds can also be seen when shorter periods are considered. For example, during a 42-h episode of favorable winds starting at 1200 UTC 23 January, data are available from buoy 3 located due east of buoy 2. The two platforms form a pair for which horizontal diffluence can be computed and compared with a similar buoy 4–FP pair located to the south. Since the shortest distance between platforms in each pair forms a line oriented almost exactly east–west, the simplest means of describing the diffluence is by calculating $\delta u/\delta x$, where δx is the distance between platforms, or 69.0 and 77.3 km for the northern and southern pairs, respectively.

The results, illustrated in Fig. 5, show that the diffluence averaged 1.2×10^{-4} s^{-1} for the two northern

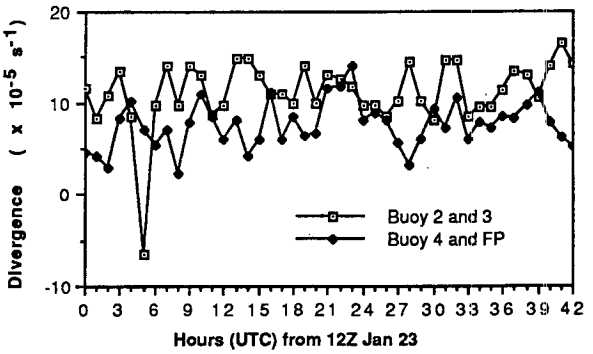

FIG. 5. The x component of the horizontal divergence of the wind computed for buoys 2–4 and FP for 1200 UTC 23 January–0600 UTC 25 January 1986.

pairs and roughly half that magnitude for their southern counterparts. Again, the persistence of the pattern is striking. Diffluence remained positive for all but one of the measurements.

4. Case studies

On 15 January, a 17-h period with north-northeast winds was accompanied by a persistent anticyclone centered over eastern North Carolina. The sea level pressure and wind fields are illustrated in Fig. 6 for 1200 UTC. The isobars are aligned roughly parallel to the coast with the strongest gradient just offshore. It is interesting that this pressure field remained fixed for the next three hours despite a large pressure increase. The isallobaric field was thus nearly uniform with a 3-h pressure increase of 3–4 mb at all locations. Thus, the anticyclone center remained stationary over land, while the strongest gradient remained along the coast.

Such a pressure pattern supports anticyclonic curvature, and thus maintains diffluence of the geostrophic wind near Cape Hatteras. If ageostrophic effects are all constant, this curvature would promote diffluence near that location, but would not explain its extension along the coastal zone to the southwest. In fact, at some locations farther southwest, the pressure field should support a slightly confluent regime.

The GALE network cannot resolve pressure patterns of wavelengths less than about 100 km over the ocean even near shore. If such patterns remain stationary, they are even harder to detect. If, however, we assume that the pressure field of Fig. 6 is not seriously aliased, the variability of ageostrophy is interesting. The wind direction at several of the nearshore platforms, such as Buoy 1, 2, and 5, and ship *NRDL* is nearly geostrophic, while farther offshore at KEOC and FP, the ageostrophy is once again large. Naturally, the resolution of the pressure pattern is poor at these more distant offshore locations, but given the reliable anchoring measurements along the coast to the south and farther offshore, it is hard to imagine that the orientation of the isobar pattern could be more than 45° in error.

The next episode of northerly winds began about one week later on 23 January and ended with the inland migration of the coastal front referred to earlier (Doyle and Warner 1990; Riordan 1990). Figure 7 illustrates conditions at 1800 UTC 24 January as the coastal front was forming in the warm waters farther to the east. Surface winds both at the coastline and farther offshore are directed from a similar north-northeast direction, while winds at the two buoys nearest shore in the bays are from the northeast and more nearly parallel to the coast. Thus, again a confluent zone lies along the coast and a diffluent zone lies farther offshore.

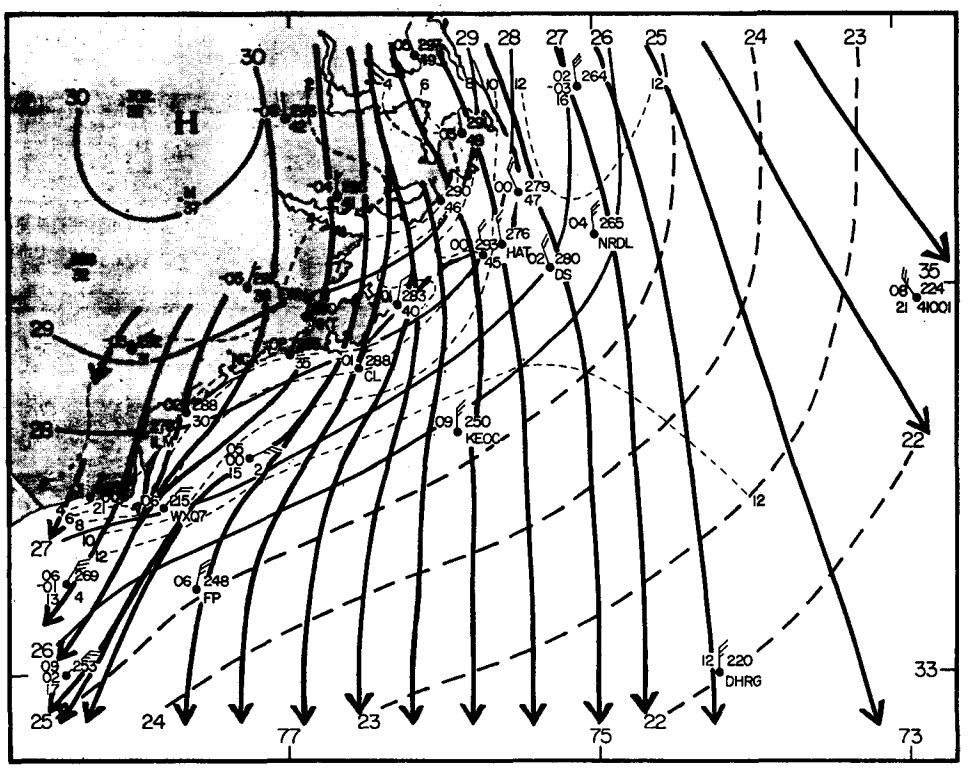

FIG. 6. Surface analysis for 1200 UTC 15 January 1986, including streamlines (thickest solid lines), sea level isobars (thinner solid and dashed lines labeled in millibars), and isotachs (very thin dashed lines labeled in meters per second).

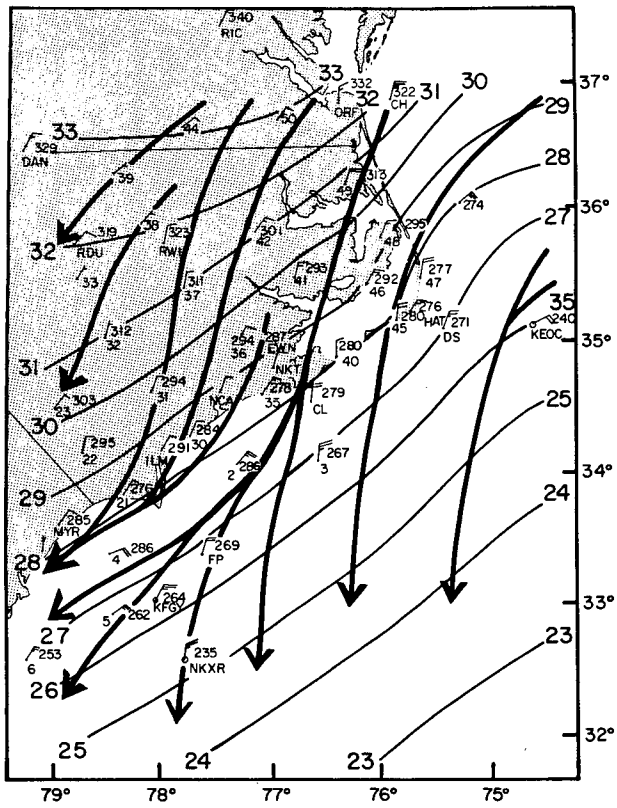

FIG. 7. Same as Fig. 6 for 1800 UTC 24 January 1986.

Some 24 h later on 25 January, the pressure field remains very similar. The isobars are aligned parallel to the coast with a strong gradient and strong north winds near shore. At about 1900 UTC the R/V *Cape Hatteras* left its home port at Beaufort, North Carolina, and traversed the region of interest, providing more detailed data than is available for most other cases. Figure 8 illustrates the resulting measurements and analysis.

Several procedures were used to allow reasonable comparison among sites. For example, since the ship traverse spans a 5-h period, data from fixed platforms are plotted as averages over the period from 1830 to 2230 UTC. Over this period at each land-based site, wind speeds showed little trend and varied within 2 m s^{-1}. Wind directions remained within 20°. At buoys 2 and 3, wind directions remained constant to within 10°, but speeds steadily increased by 2 m s^{-1}. To allow comparison with the ship wind speeds, the latter were adjusted to fit the mean linear speed trend at both buoys.

For analysis of streamlines and isotachs included in Fig. 8, all ship wind speeds were reduced by 18% to better agree with simultaneous buoy 4 measurements. The need for this adjustment is supported by the fact that, for the *Cape Hatteras,* the ship orientation with its stern toward the wind is an exposure that typically yields overestimates of ambient wind speed. Normally, ship observations are taken with the bow oriented toward the wind.

The key features of Fig. 8 are that the diffluent pattern is supported by the ship data and that the major diffluence seems to develop between buoy 3 and the ship track. Thus, major diffluence begins offshore somewhere south of Cape Lookout (site CL in Fig. 8). To the west, air parcels leaving the coast increase in speed and turn to the right. For example, the horizontal acceleration for an air parcel starting at point A attains roughly 2.3×10^{-3} m s^{-2} toward about 200° as it leaves the barrier island at about 1720 UTC. By 1900 UTC the parcel now near buoy 2 has an acceleration of roughly 0.5×10^{-3} m s^{-2} toward about 270°. The aforementioned accelerations were computed from 15-min parcel displacements from the streamline and isotach field of Fig. 8.

From air–sea temperatures and wind speeds, the sensible heat flux, computed with the bulk aerodynamic method of Large and Pond (1982), is negative landward of the 10 m s^{-1} isotach and then becomes increasingly positive offshore. By about the location of the 13 m s^{-1} isotach, the flux attains 100 W m^{-2}. These values are generally in agreement with those found earlier (Riordan 1990).

One final example of the mesoscale wind field during north-northeast synoptic-scale flow is given in Fig. 9. Here, measurements from a series of two long low-level flights of the NCAR King Air are combined with available surface data for 8 March. The aircraft data were measured at 50 m above the surface at times (UTC) given in the figure. Since these data represent conditions spanning more than a 6-h period, measurements at each fixed site are plotted for the time when the aircraft was nearest that site. The available data from ship *NLPM,* which is moving northeast, are included from 1600 to 2100 UTC. The SST field was obtained from the aircraft (solid thin lines) and supplemented by National Oceanic and Atmospheric Administration (NOAA) imagery (dashed thin lines).

The principal feature of the analysis is the strong diffluence near shore, supported largely by PAM II data and a few nearshore aircraft observations. There is some hint of weak diffluence farther offshore also, but the existence of this feature is somewhat tentative. In many ways, the case is quite different from those presented so far in that the wind along the coast is onshore from the southeast instead of strongly offshore. The existence of a sea-breeze regime is a plausible explanation, especially since the onshore flow develops during the morning as the land–sea temperature contrast becomes established (Fig. 9 inset).

5. A simple theory of flow over a heat source

In order to understand the mechanism of the mesoscale diffluent–confluent pattern as found earlier, we

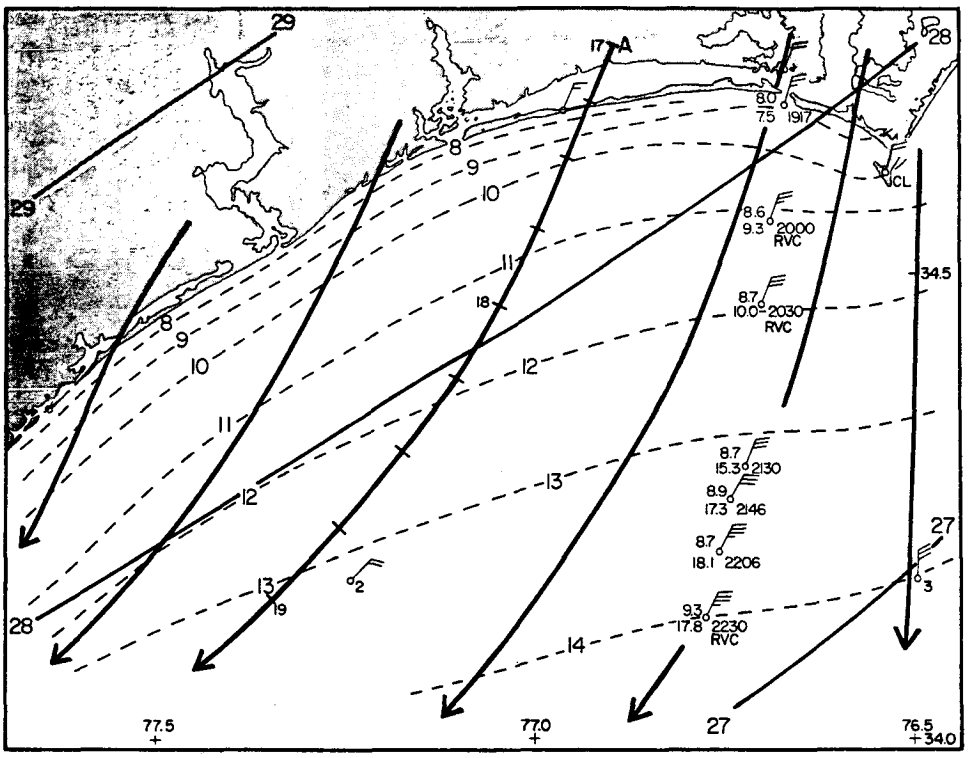

FIG. 8. Same as Fig. 6 but showing detailed surface analysis in Onslow Bay for 1830–2230 UTC 25 January. The track of the R/V *Cape Hatteras* is illustrated by the station plots labeled RVC with the times (UTC) of each observation given at the lower right of each plot. All other station plots represent average conditions. The streamline that originates over land at point *A* at 1700 UTC is marked at 15-min intervals as it extends over Onslow Bay.

develop a simple theory of a mesoscale flow over a region of prescribed heating. The heating represents the sensible heat flux associated with the temperature contrast across the continent, shelf water, and the Gulf Stream.

The governing equations for a three-dimensional, steady-state, uniform, small-amplitude, Boussinesq flow with diabatic heating may be written (e.g., see Lin 1989)

$$Lu - fv = -\pi_x \tag{2}$$

$$Lv + fu = -\pi_y \tag{3}$$

$$\pi_z = b \tag{4}$$

$$u_x + v_y + w_z = 0 \tag{5}$$

$$Lb + N^2 w = q, \tag{6}$$

where

$$L = U\frac{\partial}{\partial x} + V\frac{\partial}{\partial y} + \mu \tag{7}$$

$$q = \left(\frac{g}{c_p T_0}\right) Q. \tag{8}$$

The heating rate Q is in joules per kilogram. The kinetic pressure and buoyancy are represented by $\pi = (p/p_0)$ and b, respectively. The symbol μ represents the coefficient of Rayleigh friction in Eqs. (2) and (3) and Newtonian cooling in Eq. (6). The value of μ is assumed to be 10^{-5} s^{-1} for both Rayleigh friction and Newtonian cooling in the viscous case. Other symbols are defined as usual. Equations (2)–(6) can be combined into a single equation for w,

$$(L^2 + f^2)\frac{\partial^2 w}{\partial z^2} + N^2 \nabla_H^2 w = \nabla_H^2 q. \tag{9}$$

Making the Fourier transform of the above equation yields

$$\hat{w}_{zz} + \frac{N^2 K^2}{(kU + lV - i\mu)^2 - f^2}\hat{w} = \frac{K^2}{(kU + lV - i\mu)^2 - f^2}\hat{q}. \tag{10}$$

We assume the low-level diabatic heating decreases exponentially with height,

$$q(x, y, z) = q_0(x, y)\exp(-z/H). \tag{11}$$

Making the Fourier transform of Eq. (11) and substituting it into Eq. (10) gives

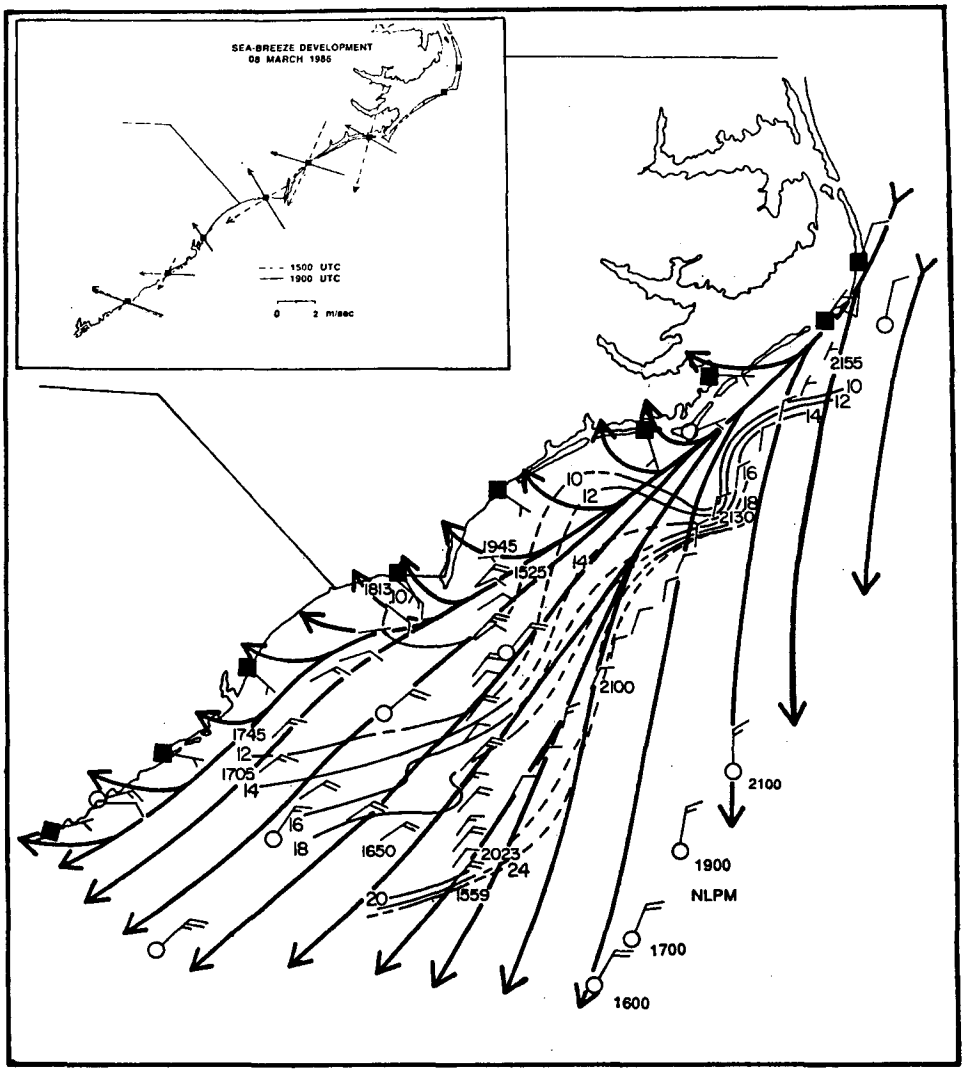

FIG. 9. Surface and 50-m aircraft winds for 8 March 1986. Data are composited from two flights of the NCAR King Air research aircraft: 1525–1813 UTC (long pendants) and 1945–2155 UTC (short pendants). Times are plotted at selected points along the aircraft route. Winds at surface sites, denoted by pendants with circles or squares, are plotted for times when the aircraft was nearest each site. Streamlines are included as heavy solid lines and SSTs (°C) as thin lines. Inset: wind vectors at coastal sites at 1500 UTC (dashed) and 1900 UTC (solid) 8 March.

$$\hat{w}_{zz} + \frac{N^2K^2}{(kU + lV - i\mu)^2 - f^2}\hat{w} = \frac{K^2}{(kU + lV - i\mu)^2 - f^2}\hat{q}_0 \exp\left(-\frac{z}{H}\right). \quad (12)$$

The general solution of the above equation can be written

$$\hat{w} = A \exp\{iNKz[(kU + lV - i\mu)^2 - f^2]^{-1/2}\} + B \exp\{-iNKz[(kU + lV - i\mu)^2 - f^2]^{-1/2}\} + \frac{H^2K^2\hat{q}_0 \exp(-z/H)}{N^2H^2K^2 + (kU + lV - i\mu)^2 - f^2} \quad (13).$$

The lower boundary condition requires the vertical velocity to be zero at the surface,

$$\hat{w} = 0 \quad \text{at} \quad z = 0. \quad (14)$$

The upper boundary condition requires $B = 0$. This will give the radiation condition for $(kU + lV)^2 > f^2$ and a bounded solution for $(kU + lV)^2 < f^2$ if the flow is inviscid (e.g., see Lin 1989). Applying (14) to (13) yields

$$\hat{w} = \frac{-H^2K^2\hat{q}_0}{N^2H^2K^2 + (kU + lV - i\mu)^2 - f^2} \times \left\langle \exp\{iNKz[(kU + lV - i\mu)^2 - f^2]^{-1/2}\} - \exp(-z/H) \right\rangle. \quad (15)$$

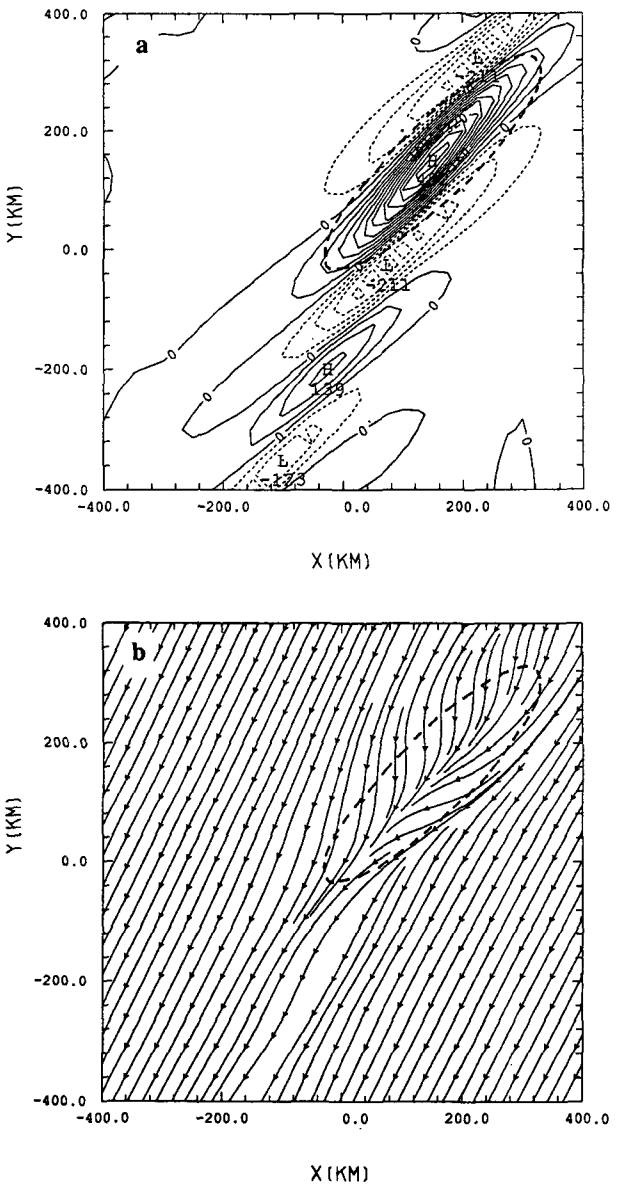

FIG. 10. (a) Vertical velocity and (b) streamlines at a height of 25 m. The solution is given in Eqs. (15)–(17) with $Q_0 = 10^{-5}$ m s^{-3}, $\alpha = 45°$, $a_x = 50$ km, $a_y = 200$ km, $U = -2.5$ m s^{-1}, $V = -5.0$ m s^{-1}, and $f = 10^{-4}$ s^{-1}. The heating rate of 2.4×10^{-6} m s^{-3} is denoted by dashed lines.

The horizontal wind velocities $\hat{u}$ and $\hat{v}$ are then obtained from the Fourier transform of Eqs. (2) and (3),

$$\hat{u} = \frac{i(fl + k\hat{L})}{\hat{L}(k^2 + l^2)}\hat{w}_z \tag{16a}$$

$$\hat{v} = \frac{i(l\hat{L} - kf)}{\hat{L}(k^2 + l^2)}\hat{w}_z, \tag{16b}$$

where $\hat{L} = ikU + ilV + \mu$. The solutions in physical space are then obtained numerically by applying the fast Fourier transform (FFT) to Eqs. (15)–(16).

Figure 10 displays the vertical velocity and streamlines at a height of 25 m for an inviscid flow over a heat source of the following function,

$$q_0(x, y) = Q_0\left[\frac{(x\cos\alpha - y\sin\alpha)^2}{a_x^2} + \frac{(x\sin\alpha + y\cos\alpha)^2}{a_y^2}\right]^{-3/2}, \tag{17}$$

with $Q_0 = 10^{-5}$ m s^{-3}, $\alpha = 45°$, $a_x = 50$ km, and $a_y = 200$ km. The e-folding value of the vertical profile of the heating is 1 km. The heating rate corresponds to a maximum sensible heat flux of about 240 W m^{-2}, which is roughly the magnitude observed during these events. The basic wind blows from the north-northeast with a speed of 5.6 m s^{-1}. Air parcels rise in the vicinity of the heating region and descend on both upstream and downstream sides (Fig. 10a). The rising motion is produced by the diabatic heating, while the descending motion is associated with the compensating downdraft (e.g., Lin and Smith 1986).

When the air parcels approach the heating region from the north, they enter the region of downward motion, which produces divergence in the horizontal velocity field as required by the incompressible continuity equation. This forces the air parcels to spread out slightly upstream of the heating region (Fig. 10b). In the heating region, the air parcels tend to converge. With the basic wind pattern, a confluent zone is produced near the heat source. Eventually, the air parcels are restored to their original direction.

To show the relative importance of the differential friction associated with the land–ocean contrast, a case was run with $\mu = 10^{-5}$ s^{-1} over the land and 0 over the ocean. The result shows that the vertical velocity decreases slightly with the differential friction included (Fig. 11a). The streamline field (Fig. 11b) is also modified slightly. The addition of differential friction, however, does not change the flow field significantly compared with the heating effect. Based on a simple physical argument, this appears reasonable also. For example, if friction suddenly decreases for air parcels moving south to Onslow Bay, as in Fig. 8, the parcels would begin an inertial oscillation with a period of about 21 h. If we assume that the parcels are in horizontal, unaccelerated flow prior to leaving the shoreline, the rapid change in friction would cause an acceleration to the right, with the velocity vector attaining a maximum rightward deviation in about 5 h. The observed deviation, however, reaches a maximum in only about 2 or 3 h.

Figure 12 displays the vertical velocity field and the streamline pattern of an inviscid flow similar to that of Fig. 10 except with a more complicated heat source. There is no differential friction included in this case. The observed pattern of surface sensible heat flux (Fig. 16, from Riordan 1990) is idealized by superimposing two bell-shaped heat sources. The heating rates of the

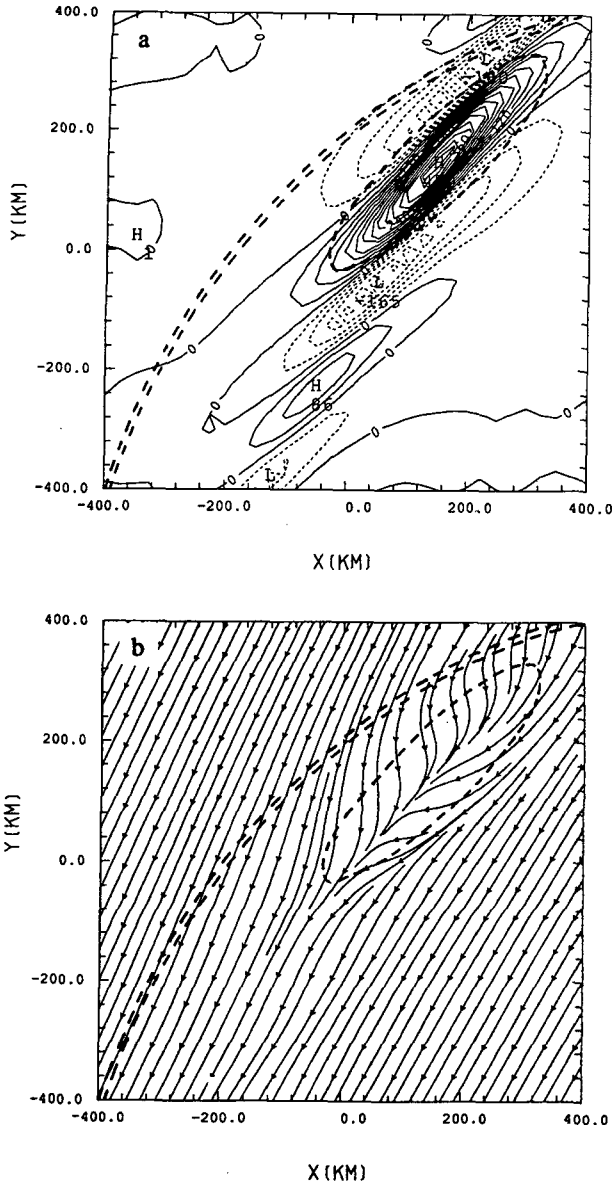

FIG. 11. Same as Fig. 10 except with the friction activated in the region to the northwest of the double-dash line. The coefficient of Rayleigh friction and Newtonian cooling is 10^{-5} s^{-1}.

northeast and southwest heat sources are 2×10^{-5} and 10^{-5} m s^{-3}, respectively. As in the case of Fig. 10, regions of upward motion exist in the vicinity of the diabatic heating. Accompanying these regions of upward motion are areas of compensating downward motion located upstream and downstream (Fig. 12a). The streamline pattern shows that two confluent zones are generated in the vicinity of the two maximum heating regions. On the west side of the northeast heat source, the air parcels turn to the right, facing downstream. This is consistent with the observed flow pattern (Figs. 4, 6, 7, and 8). Before reaching the southwest heat source, the flow diverges and then converges.

6. Summary and conclusions

A surface wind pattern characterized by stationary, persistent diffluent–confluent axes aligned parallel to the Carolina coast has been described. Appreciable upward fluxes of sensible heat from the ocean were shown to exist with the pattern.

The confluent–diffluent wind pattern appeared in virtually every case with northerly winds during the GALE winter period of about 60 days when data were available. In most cases, the confluent axis was located

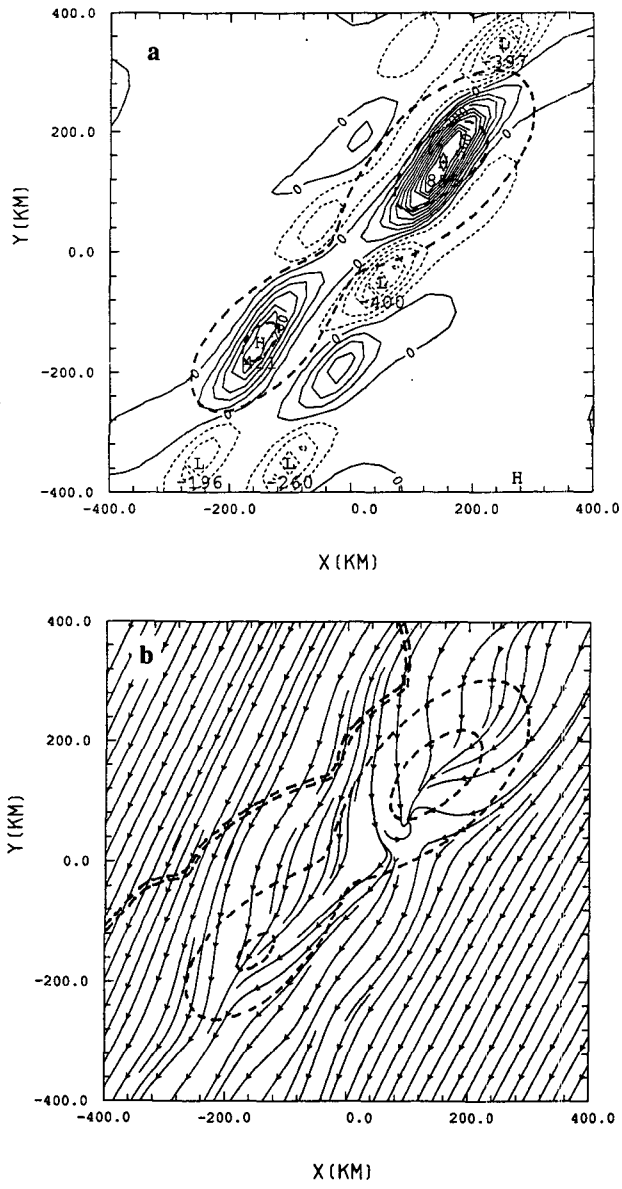

FIG. 12. Same as Fig. 10 except with two bell-shaped heating areas superimposed. The heating rates of the northeast and southwest heat sources are 2×10^{-5} and 10^{-5} m s^{-3}, respectively. Dashed lines denote contours of heating rates of 2×10^{-6} and 8×10^{-6} m s^{-3}. The approximate location of the coastline is denoted by double-dash lines in (b).

near the shoreline of Onslow Bay and Long Bay, and the parallel diffluent axis located farther offshore extended southwestward from Cape Lookout, North Carolina.

The persistence and orientation of these axes makes them important in the evolution of coastal fronts and subsequent cyclogenesis common to the region. By classical theory, frontogenesis occurs when the orientation of the axis of dilatation in the horizontal deformation field is aligned within 45° of the isotherms, while frontolysis occurs for the remaining orientations. In cases with northerly winds in winter, isotherms are typically aligned parallel to the coast. Thus, the diffluent axis would normally be frontolytic, while nearer the shore, the confluent axis would be frontogenetic. Coastal fronts typically form during northerly wind regimes and approach the nearshore waters from the east (Anderson 1991). Thus, if the pattern persists as documented, it must nearly always interact with coastal fronts.

A simple theoretical model with diabatic heating was used to simulate the flow regime. With an idealized heat source resembling the observed pattern of sensible heat flux, the main features of the flow pattern have been reproduced, namely, the diffluent band offshore and the tendency for rightward deflection of the southward-bound trajectories as they leave the coastline at Onslow Bay. The latter feature was observed only in the more complicated case that included the secondary heating region south of Onslow Bay. Thus, the model suggests that the trajectories are deflected because of the shape of the heating region offshore and that they would continue south if secondary heating centers were not observed south of the coastal bays.

In both runs of the model representing an inviscid flow over an isolated bell-shaped heat source, the air parcels rise in the vicinity of the heating center and descend on both upstream and downstream sides. In both runs, prominent confluent zones are produced over the heat source. These zones resemble the confluent bands observed over the Gulf Stream in this flow regime by Riordan (1990) and indeed suggest the convergence associated with the formative stages of the coastal front itself.

The role of the change in surface friction between land and sea was found to have little influence on the observed pattern. A model run similar to that described above—but which included frictional effects—showed little change in nearshore flow, a result consistent with simple physical arguments also. Thus, we may conclude that the diabatic heating pattern offshore, rather than differential friction, is probably the main agent producing the general flow signature observed.

Finally, caution should be used in interpreting detailed features of present model results, since the heating and flow patterns are highly idealized. For example, a more realistic boundary-layer parameterization and vertical wind shear should be considered in future model developments, which also need to reproduce the observed confluent pattern near shore.

Acknowledgments. This work would not have been possible without the dedication of many GALE scientists and support personnel. The authors especially wish to acknowledge the contributions by the mission scientists and crew aboard the NCAR King Air and the R/V *Cape Hatteras*. Special thanks also to buoy specialist Paul Blankenship. This work was funded by the National Science Foundation under Grant ATM-8807064.

REFERENCES

Anderson, J. T., 1991: Carolina coastal fronts: A case study, climatology and simple prediction scheme. M.S. thesis, Department of Marine, Earth and Atmospheric Sciences, North Carolina State University, Raleigh.

Austin, P. M., 1941: Favorable conditions for cyclogenesis near the Atlantic coast. *Bull. Amer. Meteor. Soc.*, **22,** 270–272.

Ballentine, R. J., 1980: A numerical investigation of New England coastal frontogenesis. *Mon. Wea. Rev.*, **108,** 1479–1497.

Bosart, L. F., and S. C. Lin, 1984: A diagnostic analysis of the Presidents' Day storm of February 1979. *Mon. Wea. Rev.*, **112,** 2148–2177.

Dirks, R. A., J. P. Kuettner, and J. A. Moore, 1988: Genesis of Atlantic Lows Experiment (GALE): An overview. *Bull. Amer. Meteor. Soc.*, **69,** 148–160.

Doyle, J. D., and T. T. Warner, 1990: Mesoscale coastal processes during GALE IOP 2. *Mon. Wea. Rev.*, **118,** 283–308.

Hadlock, R., and C. W. Kreitzberg, 1988: The Experiment on Rapidly Intensifying Cyclones over the Atlantic (ERICA) field study: Objectives and plans. *Bull. Amer. Meteor. Soc.*, **69,** 1309–1320.

Hsu, H.-M., 1987: Mesoscale lake-effect snowstorms in the vicinity of Lake Michigan: Linear theory and numerical simulations. *J. Atmos. Sci.*, **44,** 1019–1040.

Large, W. G., and S. Pond, 1982: Sensible and latent heat flux measurement over the ocean. *J. Phys. Oceanogr.*, **12,** 464–482.

Lettau, H. H., 1950: A re-examination of the Leipzig wind profile considering some relations between wind and turbulence in the friction layer. *Tellus,* **2,** 125–129.

——, 1962: Theoretical wind spirals in the boundary layer of a barotropic atmosphere. *Beitr. Phys. Atmos.*, **35,** 195–212.

Lin, Y.-L., 1989: Inertial and frictional effects on stratified hydrostatic airflow past an isolated heat source. *J. Atmos. Sci.*, **46,** 921–936.

——, 1990: A theory of cyclogenesis forced by diabatic heating. Part II: A semigeostrophic approach. *J. Atmos. Sci.*, **47,** 1755–1777.

——, and R. B. Smith, 1986: The transient dynamics of airflow near a local heat source. *J. Atmos. Sci.*, **43,** 40–49.

Raman, S., and A. J. Riordan, 1988: The Genesis of Atlantic Lows Experiment: The planetary-boundary-layer subprogram of GALE. *Bull. Amer. Meteor. Soc.*, **69,** 161–172.

Riordan, A. J., 1990: Examination of the mesoscale features of the GALE coastal front of 24–25 January, 1986. *Mon. Wea. Rev.*, **118,** 258–282.

Thornthwaite, C. W., W. J. Superior, and R. T. Field, 1965: Disturbance of airflow around Argus Island Tower near Bermuda. *J. Geophys. Res.*, **70,** 6047–6052.

Uccellini, L. W., R. A. Petersen, K. F. Brill, P. J. Kocin, and J. J. Tuccillo, 1987: Synergistic interactions between an upper-level jet streak and diabatic processes that influence the development of a low-level jet and a secondary coastal cyclone. *Mon. Wea. Rev.*, **115,** 2227–2261.

Whittaker, L. M., and L. H. Horn, 1982: *Atlas of Northern Hemisphere Extratropical Cyclone Activity, 1958–1977.* University of Wisconsin-Madison, 65 pp.